A&A 618, A178 (2018)
https://doi.org/10.1051/0004-6361/201732466

Astronomy & Astrophysics

(121514) 1999 UJ_7: A primitive, slow-rotating Martian Trojan⋆

G. Borisov[1,2], A. A. Christou[1], F. Colas[3], S. Bagnulo[1], A. Cellino[4], and A. Dell'Oro[5]

[1] Armagh Observatory and Planetarium, College Hill, Armagh BT61 9DG, Northern Ireland, UK
e-mail: Galin.Borisov@Armagh.ac.uk
[2] Institute of Astronomy and NAO, Bulgarian Academy of Sciences, 72, Tsarigradsko Chaussée Blvd., 1784 Sofia, Bulgaria
[3] IMCCE, Observatoire de Paris, UPMC, CNRS UMR8028, 77 Av. Denfert-Rochereau, 75014 Paris, France
[4] INAF – Osservatorio Astrofisico di Torino, via Osservatorio 20, 10025 Pino Torinese (TO), Italy
[5] INAF – Osservatorio Astrofisico di Arcetri, Largo E. Fermi 5, 50125, Firenze, Italy

Received 15 December 2017 / Accepted 7 August 2018

ABSTRACT

Aims. The goal of this investigation is to determine the origin and surface composition of the asteroid (121514) 1999 UJ_7, the only currently known L_4 Martian Trojan asteroid.
Methods. We have obtained visible reflectance spectra and photometry of 1999 UJ_7 and compared the spectroscopic results with the spectra of a number of taxonomic classes and subclasses. A light curve was obtained and analysed to determine the asteroid spin state.
Results. The visible spectrum of 1999 UJ_7 exhibits a negative slope in the blue region and the presence of a wide and deep absorption feature centred around ~0.65 μm. The overall morphology of the spectrum seems to suggest a C-complex taxonomy. The photometric behaviour is fairly complex. The light curve shows a primary period of 1.936 d, but this is derived using only a subset of the photometric data. The asteroid may be in a non-principal axis rotational state, but our observational coverage is insufficient to draw definitive conclusions.
Conclusions. Although the observed spectral absorption is wider and deeper, this finding may be compatible with the 0.7 μm spectral feature exhibited by some Ch-type asteroids and could possibly be interpreted as diagnostic of the presence of hydrated minerals. The inferred composition of 1999 UJ_7 as a primitive object can be consistent with a volatile-rich object originally accreted beyond the snow line of the solar system, and subsequently evolved to reach the inner regions of the solar system.

Key words. planets and satellites: individual: Mars – planets and satellites: individual: Trojan asteroids – techniques: imaging spectroscopy – techniques: photometric

1. Introduction

The so-called Mars Trojans are asteroids orbiting in the stability regions corresponding to the L_4 and L_5 Lagrangian points of Mars. Their existence is thought to date back to early epochs of the history of the solar system (Scholl et al. 2005). Among the nine confirmed Martian Trojans (as of 2017), eight belong to L_5 and only one, which is the subject of the present study, belongs to L_4.

Seven of the L_5 Mars Trojans are found to be members of the Eureka family that were first identified by Christou (2013) and de la Fuente Marcos & de la Fuente Marcos (2013). Recently, Borisov et al. (2017) and Polishook et al. (2017) found that the surface composition of the known Eureka family members seems to be dominated by olivine. This led Polishook et al. (2017) to suggest that these objects might be pieces of the Martian mantle, excavated from the planet's interior by a giant impact and deposited in its Trojan clouds during the late phases of terrestrial planet formation. This is currently only a speculative possibility, but in any case the inferred composition of these L_5 objects seems to correspond to what should be expected for bodies having experienced an important thermal evolution (Rivkin et al. 2003, 2007; Borisov et al. 2017). The situation may be very different in the case of asteroid (121514) 1999 UJ_7 ("UJ7" hereafter). The composition of this asteroid, the only L_4 Mars Trojan known, may have important implications for current models of early solar system evolution, as explained below. During a spectroscopic survey of Mars Trojans, Rivkin et al. (2003) obtained a visible $\lambda \in$[0.55-1.00] μm spectrum of UJ7. They interpreted the smooth, featureless spectrum as possibly diagnostic of an object belonging to the X taxonomic class. As noted by these authors, the X-class, according to both Tholen (1984) and Bus & Binzel (2002) classifications, encompasses a large variety of objects, including possible parent bodies of enstatite meteorites and iron meteorites, as well as organic-rich primitive meteorites. In the Tholen classification, the X-class is ambiguous and encapsulates three separate subclasses: E, M, and P. Uniquely assigning any one of these taxonomies to a spectrum requires independent knowledge of the albedo. The Tholen P-class was found in the 1980s to include low-albedo objects mostly orbiting in the outer main belt and in the Jupiter Trojan region (Emery et al. 2011), generally thought to have primitive, volatile-rich compositions. The low visible albedo (p_V = 0.053 ± 0.034) obtained by the NEOWISE survey (Nugent et al. 2015) might in principle be used to constrain the taxonomic classification and interpretation, but it is too uncertain to draw definitive conclusions. Interestingly enough, Rivkin et al. (2003) noted that the visible spectrum of UJ7 was also found to be similar, within

⋆ Based on service observations made with the 4.2 m *William Herschel* Telescope operated on the island of La Palma by the *Isaac Newton* Group of Telescopes in the Spanish Observatorio del Roque de los Muchachos of the Instituto de Astrofísica de Canarias and on data collected with 2 m Ritchey-Chrétien-Coudé (2mRCC) Telescope at Rozhen National Astronomical Observatory.

observational uncertainties, to that of (308) Polyxo, an asteroid belonging to the T-class defined by Bus & Binzel (2002). The T-class is also very heterogeneous in terms of possible meteorite analogues. It has been interpreted (Britt et al. 1992) as diagnostic of a troilite-rich composition, suggesting important thermal processing, because the troilite is a mineral found in mesosiderite meteorites and thought to be present in the interiors of differentiated asteroids. An alternative interpretation of the T-class is that the body surface may be composed of altered carbonaceous chondrite material (Britt et al. 1989). It is worth noting that the T-class is also considered to be a good spectral match for the leading side of the Martian satellite Phobos (Rivkin et al. 2002).

Of course, the mutually exclusive hypotheses that UJ7 could be either a thermally evolved body or a primitive object depict very different scenarios. In the former case, the properties of UJ7 would be consistent with the interpretation of Martian Trojans as surviving samples of an early population of differentiated planetesimals present in the inner solar system at the epoch of the formation of Mars (Sanchez et al. 2014). This would also provide a direct compositional link between Mars Trojans and the material in the Martian satellite system (Phobos). In contrast, a primitive composition of UJ7 would rather suggest genetic links with objects accreted in the outer solar system. This would be compatible with the hypothesis of an early inward incursion of material from the outer solar system, as predicted by recent models of early planetary evolution (Walsh et al. 2011; Vokrouhlický et al. 2016).

The limited spectral coverage and low signal-to-noise ratio (S/N) of the Rivkin et al. (2003) spectrum was not sufficient to draw robust conclusions about the most likely composition of UJ7. This motivated us to carry out new spectroscopic and photometric observations of this object to improve our understanding of its properties and obtain some more firm evidence about its most likely origin.

The paper is organised as follows. In Sect. 2 we present our observations. The data reduction procedures are described in Sect. 3, and the results in Sect. 4, separately for spectroscopy and photometry. A discussion of our results is given in Sect. 5.

2. Observations

We obtained spectra of UJ7 using the Auxiliary port CAMera (ACAM) mounted at the folded-Cassegrain focus of the 4.2 m *William Herschel* Telescope (WHT), *Isaac Newton* Group (ING) at the Roque de los Muchachos Observatory, Canary Islands on 17 Feb 2017 and using the 2-channel focal reducer (FoReRo2) of the 2 m Ritchey-Chrétien-Coudé (2mRCC) Telescope at the Bulgarian National Astronomical Observatory (BNAO), Rozhen on 25 Dec 2016. Photometric observations were carried out using both FoReRo2 and the CCD camera at the 1 m telescope (T1m) at the Observatoire Midi-Pyrénées (OMP) situated on the technical platform of the Pic du Midi observatory, on the following six nights: 1, 2, 5, 6, and 29 Dec 2016 and 1 Jan 2017, when the asteroid was at heliocentric distance $r = 1.48$ au and geocentric distance $\Delta = 0.63$ au and its phase angle changes from 30 to 27 degrees. A Sloan r′ filter was used. Details of our observations are shown in Tables 1 and 2.

2.1. Spectroscopy

2.1.1. ACAM

The low-resolution spectroscopy mode of ACAM was used for high-throughput low-resolution spectroscopy in the range 3500–9400 Å . On-axis resolution at 6000 Å is $R \sim 450$ and 900 for 1.0- and 0.5-arcsec slits, respectively. We used a GG495 order-blocking filter to obtain a region uncontaminated by light from other orders from 4950 to 9500 Å[1]. The solar analogue HD 28099 was observed to calibrate the asteroid spectrum.

Table 1. Spectroscopic observations.

Object	Date	UT	Air mass	App. V_{mag}	Exp. T N × (s)	Instrument
UJ7	17 Feb 2017	02:00	2.00	19.04	2 × 600	ACAM
HD 28099	17 Feb 2017	00:20	2.13	8.12	1 × 5	
UJ7	25 Dec 2016	03:05	1.49	18.11	2 × 600	FoReRo2
HD 86728	25 Dec 2016	03:54	1.09	5.40	1 × 2	

2.1.2. FoReRo2

The instrument adapts the imaging elements of the detector to the characteristic size of the object or the seeing disc. Built mainly for observations of cometary plasma, FoReRo2 has proven to be suitable for many other tasks (Jockers et al. 2000). This instrument allows long-slit spectroscopy with a Bausch & Lomb grating prism, working in the parallel beam of FoReRo2, with 300 lines mm^{-1} giving a spectral resolution of 4.3 Å px^{-1} using a 200 μm slit width or 2.6 arcsec on the sky. The solar analogue HD 86728 was observed to calibrate the asteroid spectrum.

2.2. Sloan r′ photometry

2.2.1. FoReRo2

The imaging mode of the instrument was used for photometry of UJ7. For this investigation we used a Sloan r' filter, therefore only the red channel of the instrument was in operation.

2.2.2. T1m

The observations were performed with a DZ936BV Marconi CCD, using the same Sloan r' filter.

3. Data reduction

3.1. Spectroscopy – ACAM and FoReRo2

All spectra were reduced under the assumption of point-like sources and had their instrument signature removed by debiasing, flat-fielding, wavelength calibration, signal extraction, and sky subtraction with the IRAF packages CCDRED and ONEDSPEC.

To maximise the S/N, the reduced 1D spectra for both the asteroid and solar analogue stars were rebinned in 7.5 nm steps, which is 22 times coarser than the spectrograph resolution (~0.34 nm px^{-1}), after applying a σ-clipping cleaning algorithm in the same wavelength window. The asteroid spectrum was then divided by the solar analogue spectrum and the result was normalised to unity at $\lambda = 550$ nm. For FoReRo2, we used different rebinning steps in the blue and red parts of the spectra at 7.5 and 30 nm, respectively, to account for the lower S/N ratio at

[1] Details of ACAM spectroscopy are available at the ING website: http://www.ing.iac.es/Astronomy/instruments/acam/spectroscopy.html.

Table 2. Photometric observations.

Date	UT	Air mass	App. V_{mag}	Filter	Exp. T $N \times$ (s)	Instrument
05 Dec 2016	16:50	1.946				
|	|	1.101	18.20	r'	295 × 120	
06 Dec 2016	04:35	1.384				
06 Dec 2016	18:20	1.565				FoReRo2
|	|	1.102	18.19	r'	255 × 120	
07 Dec 2016	04:35	1.398				
01 Jan 2017	19:00	1.137				
|	|	1.085	18.15	r'	240 × 120	
02 Jan 2017	04:40	2.106				
01 Dec 2016	21:30	1.361				
|	|	1.085	18.20	r'	340 × 90	
02 Dec 2016	06:15	1.325				
02 Dec 2016	19:30	1.699				CCD@T1m
|	|	1.086	18.19	r'	390 × 90	
03 Dec 2016	05:30	1.252				
29 Dec 2016	17:55	1.420				
|	|	1.081	18.15	r'	235 × 90	
30 Dec 2016	00:25	1.113				

longer wavelengths. The spectral range used for analysis was selected to be $\lambda > 0.53\,\mu$m, because of the transmittance curve of the GG495 order-blocking filter and $\lambda < 0.88\,\mu$m, because of strong fringing above this wavelength. The resulting spectra are shown in Fig. 1. Regions with strong H_2O and O_2 telluric absorption are indicated with ⊢ symbols in the bottom of the plot shown in the left panel, showing the reflection spectrum obtained at WHT. We included these wavelength intervals in the analysis because the general trend of the spectrum is not dramatically affected by these regions. In spite of an aggressive binning, measurement uncertainties remain considerable in the FoReRo2 data, especially at wavelengths longer than 0.7 μm. However, we note that both spectra show a strong negative slope shortward of 0.65 μm where the S/N is highest; this bolsters confidence that the WHT spectrum, in particular, is reliable and does not suffer from significant systematic effects.

3.2. Photometry – FoReRo2 and T1m

All imaging data had their instrument signatures removed the same way as the spectral data. Standard DAOPHOT aperture photometry with aperture size of $2 \times FWHM$ was performed. Standard stars in the field of view from the APASS [2] catalogue were used for absolute calibration.

4. Results

4.1. Taxonomy

We determined the taxonomy of UJ7 by applying (i) slope-fitting and (ii) χ^2 goodness-of-fit ranking based only on the ACAM spectrum (left panel of Fig. 1) because the Rozhen spectrum is of a much poorer quality.

First, we estimated the slope γ of the spectrum by fitting a function of the form $r = 1.0 + \gamma(\lambda - 0.55)$ to the data, where λ is the wavelength in μm (Bus & Binzel 2002). The best-fit slope was found to be $\gamma = -0.378^{+0.024}_{-0.025}\ \mu\text{m}^{-1}$; this value is consistent with, although at the high end of, a B-class taxonomy, which is a subgroup of the big, low-albedo C-complex (Bus & Binzel 2002). These asteroids are generally thought to be primitive, volatile-rich or aqueously altered remnants from the early solar system. Although we computed the slope based on a slightly narrower (≳70%) wavelength range than in Bus & Binzel, the resulting value is not affected by a large uncertainty. As noted above, the NEOWISE survey (Nugent et al. 2015) obtained a low geometric albedo value of 0.053 ± 0.034 and a diameter of 2.29 ± 0.49 km for this asteroid. In spite of its relatively large albedo uncertainty, the nominal albedo value is consistent with a C-complex classification.

The next step was to compute curve matching of the obtained spectrum using all known taxonomic classes from Bus & Binzel (2002). Table 3 shows the top five matches using the cost functions (Popescu et al. 2012)

$$\chi^2_\mu = \sum_i^N \frac{e_i^2}{\mu_i}, \qquad \Phi_{\text{std}} = \frac{1}{N}\sqrt{\sum_i^N (e_i - \bar{e})^2}, \tag{1}$$

where $e_i = x_i - \mu_i$ and $\bar{e}$ its mean value, x_i is the measurement at the i^{th} wavelength position, and μ_i is the model evaluation at the same location.

Both cost functions assign the highest rankings to the C-complex taxonomies, including the C-class itself and its four distinct subclasses Ch, Cb, B, and Cgh. The Ch class was found to give the best match of our data. The ranking order is different for the remaining four places. In particular, the χ^2_μ assigns the second place to the B taxonomy, while Φ_{std} assigns B to the fifth place.

A comparison of the UJ7 spectrum with average spectra for the Ch, B, and Cgh classes is shown in the left panel of Fig. 2. The spectra of representative asteroids of the same classes as the top five matches presented in Table 3 are compared with UJ7 spectrum as well (see the left panel of Fig. 2). UJ7 exhibits a strong absorption feature centred shortward of 0.7 μm. This bears some resemblance with a feature seen in Ch and Cgh spectra, but in the case of UJ7 we have a much wider and deeper absorption feature and a maximum depth is located at a somewhat shorter wavelength. The exact morphology (centre, depth, and width) of this spectral feature tends to vary a little according to a more or less aggressive smoothing of the data. We find that the centre of the absorption for different smoothing options is between 0.65 and 0.68 μm, so it is only weakly dependent on data smoothing. In any case, we find that this spectral feature is too wide and sharp to be a spurious telluric line artefact (see Fig. 1).

The presence of a 0.7 μm feature on asteroid spectra has been considered by many authors as diagnostic of the presence of hydrated minerals on the surface (Lebofsky 1980; Vilas & Gaffey 1989; Vilas et al. 1994). Among the asteroids plotted as a comparison in the right panel of Fig. 2, (19) Fortuna (Ch-class) bears a better resemblance to our spectrum of UJ7. The absorption feature seen in Fortuna's spectrum, however, is significantly shallower than in the case of UJ7, although it seems to be centred at a similar wavelength, shortward of 0.7 μm. A much narrower absorption feature, centred around 0.7 μm, can be seen also in the spectrum of the Cgh-class asteroid (776) Berbericia, but the drop-off shortward of 0.6 μm is not present in this case, nor in the case of the spectrum of (1) Ceres, which is also shown in the figure. To summarise, the reflectance spectrum of UJ7 bears some resemblance with the Ch subclass of the C-complex, but in some respects UJ7 might represent a new and previously unknown case that can possibly be interpreted as the prototype of a new subclass.

[2] https://www.aavso.org/apass

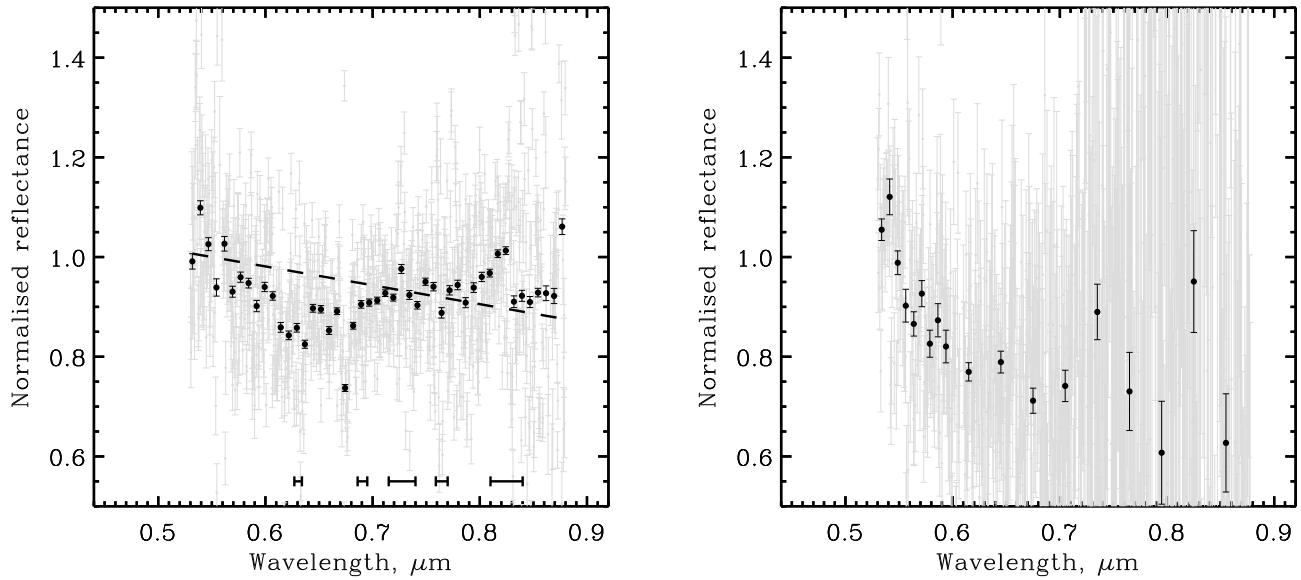

Fig. 1. Reflectance spectra of the asteroid (121514) 1999 UJ7. *Left panel*: reduced spectrum (grey) and the same data rebinned in 7.5 nm steps (black) obtained with ACAM at WHT. Regions with strong H_2O and O_2 telluric absorption are denoted with ⊢. *Right panel*: spectrum obtained with FoReRo2@2mRCC. See text for details.

Table 3. Taxonomic ranking of the UJ7 spectrum.

Taxonomic class	χ^2_μ	Taxonomic class	$\Phi_{\rm std}$
Ch	0.326	Ch	0.0064
B	0.377	Cb	0.0068
Cgh	0.459	Cgh	0.0072
Cb	0.478	C	0.0075
C	0.496	B	0.0083

The smoothed data on Fig. 2 is used just to show the global trend of the UJ7 spectrum and to find a better normalisation factor for the noisy data, but not for taxonomic ranking. The smoothing was carried out using least-squares (Savitzky–Golay) polynomial smoothing filter applied to the binned spectrum using the IDL routine POLY_SMOOTH from NASA IDL Astronomy User's Library[3].

Of course, we cannot firmly state that the absorption feature observed in UJ7 must be forcedly considered as diagnostic of water of hydration. We note, however, that the 0.7 μm feature detected in asteroid spectra varies considerably in different cases, typically between 0.67 and 0.72 μm for the location of its centre, and between 1% and 4% in depth. In some individual cases, it can reach locations down to 0.65 μm and depths up to 6% (see Fornasier et al. 2014, Fig. 13). A tentative interpretation of our data may therefore be that the observed feature is diagnostic of the presence of hydrated minerals, and its unusual attributes may be only partly due to incomplete telluric line removal combined with the coarse resolution of the spectrum.

The peculiar properties of the strong absorption feature found in the UJ7 spectrum can be thoroughly real and represent a first example of a previously unknown subclass of the C-complex. This might be related to the extended residence time of this asteroid at 1.5 au, namely closer to the Sun than any classical main belt asteroid.

[3] https://idlastro.gsfc.nasa.gov

Laboratory experiments in which meteorite powders were subjected to varying degrees of heating show that this feature is destroyed at temperatures >400 °C (Hiroi et al. 1996). Assuming energy balance, a typical subsolar point temperature for UJ7 is $T = [(1-A) * S/\eta\epsilon\sigma]^{1/4}$ (Lebofsky & Spencer 1989), where A is the Bond albedo; S the solar energy influx $S = S_0/a^2$, where S_0 is the solar constant; a the semi-major axis of the asteroid; η the beaming parameter; σ Boltzmann's constant; and ϵ the infrared emissivity. Nugent et al. (2015) obtained $\eta = 0.95 \pm 0.18$ for this asteroid by applying the Near Earth Asteroid Thermal Model (NEATM; Harris 1998) to NEOWISE survey data. Although we are aware of alternative, potentially more accurate, methods to constrain asteroid surface properties from thermal observations (e.g. Lebofsky et al. 1986; Spencer 1990), we adopted the NEATM values for p_V and η as they are obtained self-consistently from the model. Likewise, we adopt $\epsilon = 0.9$ to maintain consistency with the NEATM.

For $a = 1.52$ au, $A = 0.393 p_V$ (Eqs. 33 and A7 of Bowell et al. 1989, where we have used $G = 0.15$) and η equal to the Nugent et al. (2015) value, we obtain $T = 331$ K. An alternative thermal solution that uses WISE W3 and W4 band data (Mainzer et al. 2012) in addition to the W1 and W2 band data used in Nugent et al. (2015) is reported in Alí-Lagoa & Delbo (2017), giving $p_V = 0.041$ and $\eta = 1.08$. Carrying out the same calculation as above, we obtain a slightly lower temperature, 321 K. In any case, this temperature varies depending on the eccentricity history of the orbit; for $e \lesssim 0.1$ expected for stable Martian Trojans the variation may be as high as 302−368 K if we also consider the reported 1σ uncertainty for η in Nugent et al. (2015). Therefore, the presence of a water-of-hydration feature on UJ7 is consistent with this primitive body having been in its present orbit or further from the Sun for ~4 Gyr.

For completeness, we also note that a feature at 0.654 μm has been identified in spectra of Phobos and Deimos by Fraeman et al. (2014). Those authors obtained a best-fit model of the feature for a mixture of iron particles of various sizes embedded in a neutral silicate matrix. That feature was superimposed on a red-sloped continuum that is not apparent in our data, therefore we consider this a less likely interpretation for the UJ7 spectrum.

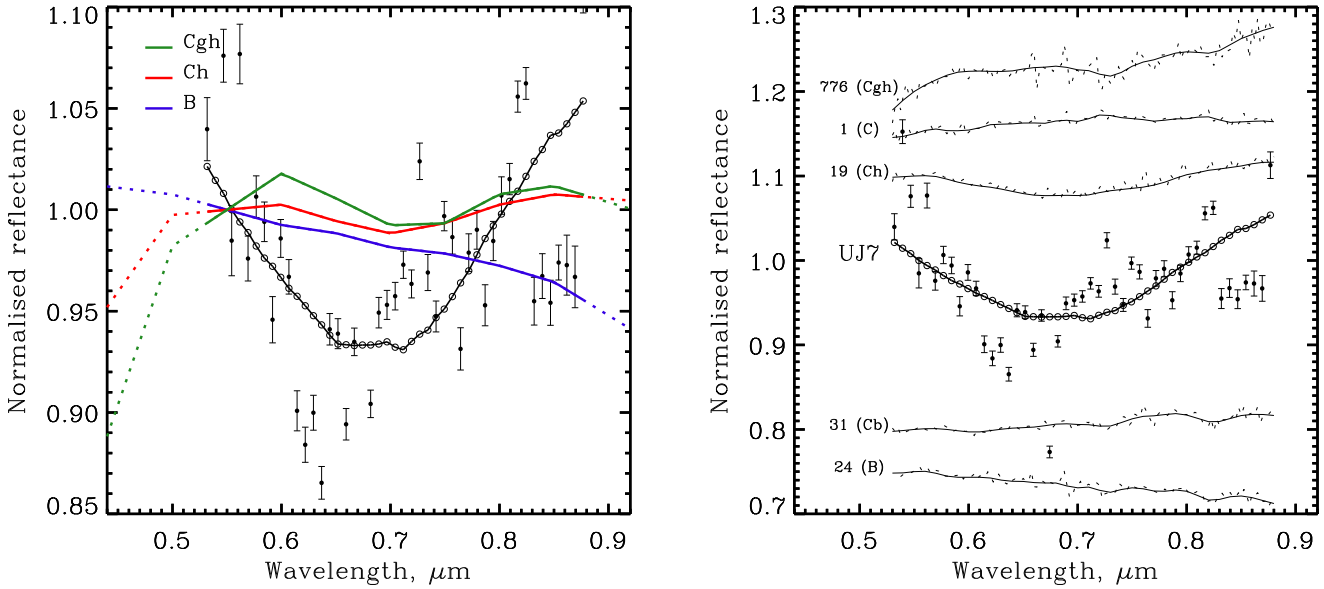

Fig. 2. *Left panel*: average spectra of Ch, Cgh, and B classes from Bus & Binzel (2002) (red, green, and blue lines, respectively) together with the binned spectrum of UJ7 (black dots). The solid colour lines show the observed wavelength coverage of the average database spectra and the solid line with open circles represents least-squares (Savitzky–Golay) polynomial smoothing filter with window width equal to 47 of the observations. *Right panel*: comparison of the UJ7 spectrum (the same binned and smoothed as on the *left panel*) with spectra of other asteroids (thin lines and dots) belonging to the taxonomic classes in Table 3. The spectra of the various asteroids represented in this figure are all normalised to 0.55 μm, but each spectrum (apart from that of UJ7) has been shifted up or down by some amount for the sake of clarity.

The authors found a few asteroids in the Vilas asteroid spectral catalogue (Vilas et al. 1998) that have the same absorption feature that is also superimposed on the red-sloped continuum. They ascribe this feature to Fe-bearing phyllosilicates that are almost always accompanied by additional absorption at 3 μm associated with hydration or hydroxylation. Interestingly, all these asteroids are further away than 3 au, which may point us to a possible origin of UJ7.

4.2. Spin state

To determine the spin rate of the asteroid, the time series of the absolute calibrated magnitude of UJ7 was fitted to a harmonic function. We used a single-period Fourier series of the form

$$F^m(t) = C_{00} + \sum_{j=1}^{m} \left[C_{j0} \cos \frac{2\pi j}{P_\psi} t + S_{j0} \sin \frac{2\pi j}{P_\psi} t \right], \quad (2)$$

where m is the series order (we used third order), C_{00} is the mean reduced magnitude, C_{j0} and S_{j0} are the Fourier coefficients, P_ψ^{-1} represents the frequency, and t is the time.

We did not succeed to obtain a satisfactory fit to the entire dataset, so we divided the data into two groups: one for early and the other for late December and fit these separately. This yielded periods of 1.936 d for the early December and 1.848 d for the late December data (Fig. 3). We note that the model light curves appear different for the two fits.

Plotting the χ^2 statistic (Fig. 4), we find that the fit for the late December data is somewhat shallow and broad compared to that for early December; the latter solution lies within 1σ of the former. This suggests that the period is constrained mainly from the early December data. We tested this by again fitting the late December data but using a fixed value $P = 1.936$ d for the period while allowing the remaining parameters to vary in the fit (right panel of Fig. 3 and see caption). Although the fit itself is satisfactory, the best-fit model appears, not unexpectedly, to be significantly different, in terms of light-curve morphology, with respect to what was previously. A simple explanation might be that the late December dataset is, by itself, insufficient to constrain the light-curve parameters. On the other hand, if this was the case, and the period derived by the only early December data was correct, we could not explain the difficulty encountered in fitting all the data together. It seems rather that there is some significant change of morphology of the light curve taking place in only a few weeks. A possible reason could be the interplay of an asymmetrical shape and a change of aspect angle of the asteroid (the angle between the rotational axis and line of the sight). It was shown long ago (Cellino et al. 1989) that significant changes in light-curve morphology can be due to shape effects in a large variety of cases. On the other hand, the time span between the first and the last observations seems too short to justify big light-curve morphology changes. Another possibility is that a change in the rotational state of the asteroid may have occurred over an interval of ~1 month, implying that the asteroid is not in principal-axis (PA) rotation. In Fig. 5 we show spin rate versus diameter for more than 10 000 asteroids[4]. All non-principal-axis (NPA) and PA rotation asteroids with known spin rate and size are also presented with green squares and blue triangles, respectively. The straight lines illustrate damping timescales of 4.5, 1, and 0.1 (bottom to top) for NPA rotation using the relation $P \approx CD^{2/3}\tau^{1/3}$ from Harris (1994), where $C \sim 17$ (uncertain by a factor of ~2.5), P is the rotation period in h, D the diameter in km, and τ the damping timescale in billions of years. Plotting the position of the asteroid on this diagram shows that UJ7 is found near the NPA rotators and near some of PA rotators, but also near 4.5 by damping timescale line. The possibility that this asteroid can be an NPA rotator cannot be ruled out for an object of its size. This would explain the

[4] JPL Solar System Dynamics Database: https://ssd.jpl.nasa.gov/sbdb_query.cgi

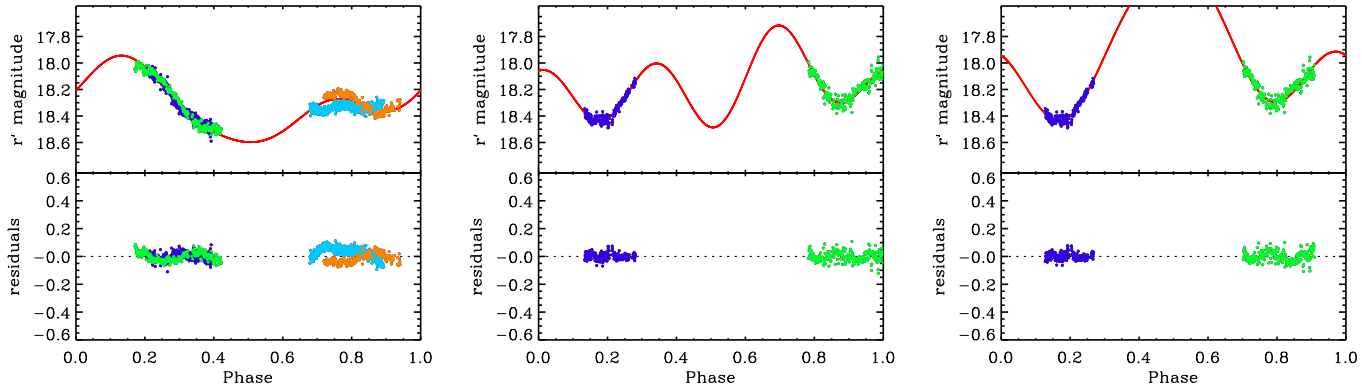

Fig. 3. Fourier fits to the photometric data of the asteroid (121514) 1999 UJ7. Different colours correspond to data from different nights. *Left panel*: light curve with fitted third-order Fourier polynomial in red (*top panel*) and the residuals (*bottom panel*) using data from 1, 2, 5, and 6 Dec 2016. The obtained period is 1.936 ± 0.002 d. *Middle panel*: as for the *left panel*, but fitting data from 29 Dec 2016 and 01 Jan 2017. The obtained period in this case is 1.848 ± 0.028 d. *Right panel*: as in middle panel, but keeping the period fixed at $P = 1.936$ d.

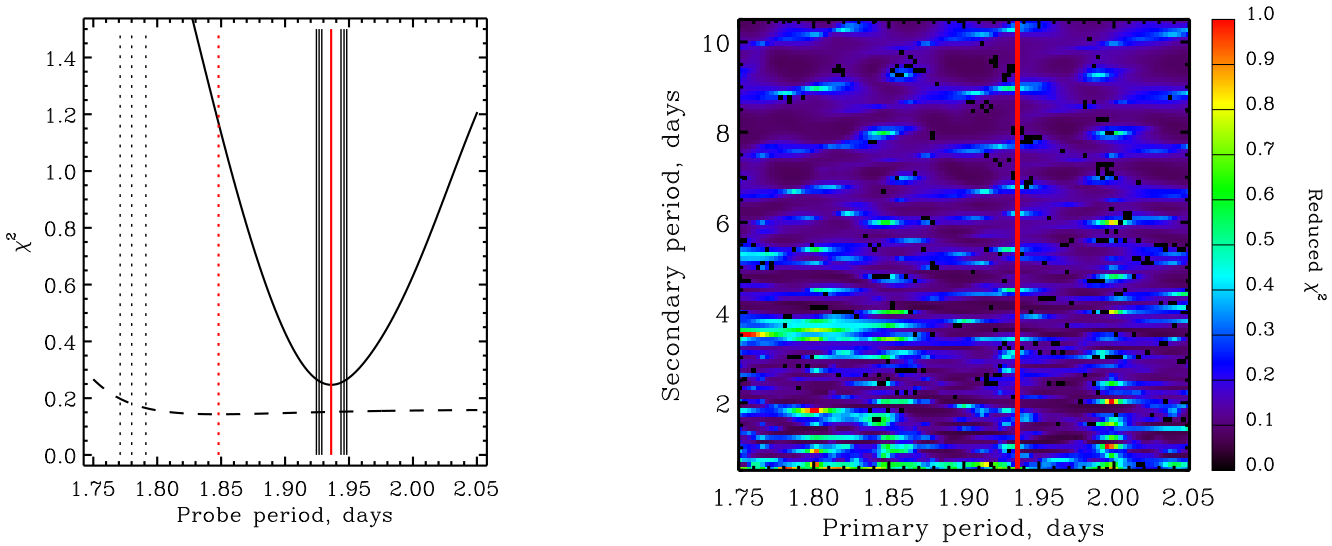

Fig. 4. *Left panel*: χ^2 of a Fourier polynomial fit varying the period between 1.75 and 2.05 d. The solid curve represents results from fitting data from 1, 2, 5, and 6 Dec 2016, while the dashed curve uses data from 29 Dec 2016 and 01 Jan 2017. The red solid and dotted vertical straight lines indicate best-fitted periods of 1.936 ± 0.002 and 1.848 ± 0.028 d, respectively. The black solid and dotted lines represent 1, 2, and 3σ uncertainties for each fit as follows: ± 7.5, $^{+9.6}_{-9.9}$, and $\pm 12 \times 10^{-3}$ d. *Right panel*: χ^2 distribution for a two-period Fourier polynomial fit. The single-period solution of 1.936 d is indicated by the vertical red line.

difficulty in obtaining a good single-period fit for the entire one-month data arc. On the other hand, we have to stress that the location of UJ7 in the spin rate – size plot cannot be a strong argument, suggesting only a partial indication about it. The NPA rotation implies the presence of a secondary period in the light curve. Therefore, we searched for a two-period solution by fitting a Fourier series as in Pravec et al. (2005) while scanning through solution space for primary and secondary periods in the domain $[1.75, 2.05] \times [0.5, 10.5]$ d. The distribution of χ^2 for this search is shown in the right panel of Fig 4. Several local minima are apparent but no single solution stands out. In conclusion, we are unable to confirm that this asteroid is in an NPA rotational state; a definite answer to this question will require better observational coverage of its light curve.

5. Discussion

Rivkin et al. (2003) classified the asteroid as X-class based on a featureless spectrum of positive visible slope (their Fig. 6). Our spectrum, however, shows a clearly negative slope at the shortest wavelengths. Our results confirm the Rivkin et al. conclusion that the mineralogy of UJ7 is unlike that of its neighbours at L_5. However, our new spectrum supports a spectral classification that is consistent with the NEOWISE visible albedo, suggesting that this asteroid has suffered minimal to no thermal, or geological, processing since the epoch of its formation.

The difference between our spectrum and that obtained in the past by Rivkin et al. (2003) might be possibly interpreted as evidence for rotational variability across the surface of the asteroid. Visible slope variability has also been documented for C-complex near-Earth objects: (153591) 2001 SN_{263} ($D = 1$ km, Perna et al. 2013), where the slope varies from flat to strongly negative (their Fig. 2) and (175706) 1996 FG_3 (Perna et al. 2014, $D = 1.7$ km), where the slope varies from positive to weakly negative (their Fig. 3). In addition, a set of Main Belt asteroids investigated by Fornasier et al. (2014) also shows some significant slope variability in the visible region (their Table 5), even for different spectra acquired from the same asteroid, as in the case of (1467) Mashona, showing both a positive and a negative

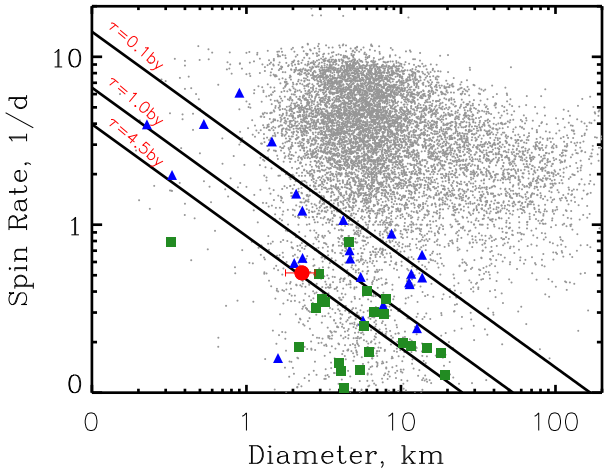

Fig. 5. Asteroid spin rate vs. diameter. The datum for UJ7 is presented as a red dot. All NPA and PA asteroids with known spin rate and size are presented with green squares and blue triangles, respectively. The lines represent damping timescales of 4.5, 1, and 0.1 (bottom to top) for NPA rotation.

slope. Therefore, a strong rotational dependence of the spectral slope for UJ7, while unusual, is not unprecedented.

Binzel et al. (2015) interpreted variability in the observed spectral slope of asteroid (109155) Bennu, target of the OSIRIS-REx mission, in terms of regolith grain size variations across its surface. According to their model, the observed spectral slope would depend on the existence of an equatorial ridge created by a YORP spin-up. In the case of UJ7, however, the slow rotation argues against the existence of such a ridge.

The spectral slope of primitive asteroid surfaces may also be modified by space weathering (Moroz et al. 1996; Lantz et al. 2013; Matsuoka et al. 2015). In this context, the existence of surface units of different colours would imply a resurfacing mechanism at work, perhaps a cratering impact that created a patch of fresh material on the surface of UJ7.

The difference between our spectrum of UJ7 and the spectrum obtained in the past by Rivkin et al. (2003) might be due to some spurious effect, which is unlikely because the spectral feature is very similar observed with both the ACAM and FoReRo2 instruments. In this case, however, we do not deal with a simple difference in the spectral slope, but we have a different overall morphology of the reflectance spectrum.

Ch- and Cgh-type asteroids may typically display a sharp spectral feature at ~3 μm (Takir & Emery 2012). These asteroids are considered to be likely parent bodies of the most common class of hydrated meteorites, namely CM chondrites (Vernazza et al. 2016, and references therein). Unlike other CC meteorites, the CM parent bodies seem to have experienced only mild heating (<400 °C) during their lifetime to preserve the 0.7 μm feature. The ~3 μm feature survives heating up to 700 °C (Hiroi et al. 1996), therefore in the case in which the absorption band in the spectrum of UJ7 is due to the presence of hydration, we can predict that this asteroid should also exhibit a ~3 μm absorption feature; this hypothesis can be verified or contradicted by future observations in the IR.

At the same time, we consider it unlikely that this asteroid has retained any traces of its original cache of volatiles in its interior. The characteristic timescale to achieve a uniform temperature throughout the asteroid is $t_h = \frac{1}{12}(D\rho C/\Gamma)^2$, where D is the diameter, Γ the thermal inertia, ρ the bulk density, and C the specific heat capacity (Busarev et al. 2018). For $D = 2300$ m, $\Gamma = 200$ J K^{-1} m^{-2} s$^{-1/2}$, $\rho = 1300$ kg m^{-3}, and $C = 600$ J kg^{-1} K^{-1}, we obtain $t_h \simeq 2 \times 10^5$ yr, which is four orders of magnitude shorter than the likely residence time of the asteroid at 1.5 au.

According to the so-called Grand-Tack (Walsh et al. 2011) model of the early solar system evolution, volatile-rich planetesimals originally accreted between and beyond the original orbits of the giant planets were scattered inwards and became embedded into the asteroid belt as a consequence of a complicated path of migration of Jupiter. Water ice that has been detected on the surfaces of outer belt asteroids (Campins et al. 2010; Rivkin & Emery 2010; Licandro et al. 2011) and objects of similar composition may have been responsible for the delivery of water to the Earth (Morbidelli et al. 2000, 2012; Izidoro et al. 2013; Raymond & Izidoro 2017). On the other hand, Polishook et al. (2017), in arguing for a Martian origin for most of the L$_5$ Mars Trojans, showed that Mars Trojans were efficiently locked into place during the final stages of terrestrial planet formation, when encounters with planetary embryos may have caused chaotic wandering of the Martian orbit. Therefore, the existence of a member of the C-complex located in L$_4$, as concluded from the spectral slope and taxonomic matching, constitutes direct evidence for the presence of geologically unprocessed objects not originating in the region of accretion of Mars, as opposed to the case of the Eureka family (Polishook et al. 2017) in L$_5$. In this context, a possible hypothesis is that UJ7 may have originated in a region near or beyond the snow line. During the early chaotic phases predicted by the Grand Tack model, it may have been perturbed in such a way as to finally achieve a low-eccentricity orbit at 1.5 au, where it was eventually captured as a permanent Mars Trojan when the planetary embryos in Mars-crossing orbits started to disappear. In particular, it is known that after the phase described by the Grand–Tack model, many small objects present in the outer regions of the solar system continued to be subject to strong perturbations, until the end of the so-called Late Heavy Bombardment era. This epoch of transition between the early planetary migrations and the final establishment of the outer planets in their current orbital locations is described by the so-called Nice model (Desch 2007). An important implication of the scenario described above is that the original influx of C-complex asteroids moving into Mars-like orbits must have been not only significant, if we consider that the estimated mass of UJ7 accounts for ~50% of the current total mass budget in the Trojan clouds, but also took place in very early epochs when the capture of objects into Trojan orbits was easier.

Regarding future observational prospects, the next two apparitions of UJ7 in 2018/19 and 2020/21 are slightly more favourable than in 2016/17. The asteroid will be at $V < 18$ at its brightest. Observation modes such as spectroscopy requiring long dwell times are facilitated during periods when the asteroid is near stationary. For UJ7, this did not occur in 2016/17 but will occur in Dec 18/ Jan 19 and April/May 21, respectively. High S/N spectroscopy both in the visible and the near-IR would allow the search for additional evidence of hydrated minerals and would better constrain the surface heterogeneity with respect to what was done in this work and by Rivkin et al. (2003). Furthermore, additional photometric coverage will be important to confirm a possible complex rotational state of this asteroid. Finally, our understanding of UJ7 and other similar asteroids will presumably benefit from the ongoing Hayabusa 2 and OSIRIS-REx missions, which will conduct in situ investigations and return samples from two C-complex asteroids: (162173) Ryugu and (101955) Bennu (Clark et al. 2011; Perna et al. 2017).

Acknowledgements. This work was supported via a grant (ST/M000834/1) from the UK Science and Technology Facilities Council. The 4.2 m *William Herschel* Telescope and its service programme SW2016b13 are operated on the island of La Palma by the *Isaac Newton* Group of Telescopes in the Spanish Observatorio del Roque de los Muchachos of the Instituto de Astrofísica de Canarias. We gratefully acknowledge observing grant support from the Institute of Astronomy and Rozhen National Astronomical Observatory, Bulgarian Academy of Sciences. This research was made possible through the use of the AAVSO Photometric All-Sky Survey (APASS), funded by the Robert Martin Ayers Sciences Fund. This publication also makes use of data products from NEOWISE, which is a project of the JPL/California Institute of Technology, funded by the Planetary Science Division of NASA.

References

Alí-Lagoa, V., & Delbo, M. 2017, A&A, 603, A55
Binzel, R. P., DeMeo, F. E., Burt, B. J., et al. 2015, Icarus, 256, 22
Borisov, G., Christou, A., Bagnulo, S., et al. 2017, MNRAS, 466, 489
Bowell, E., Hapke, B., Domingue, D., et al. 1989, in Asteroids II, eds. R. P. Binzel, T. Gehrels, & M. S. Matthews (Tucson, AZ: University of Arizona Press) 524
Britt, D. T., Bell, J. F., Haack, H., & Scott, E. R. D. 1989, in Asteroids II eds. R. P. Binzel, T. Gehrels, & M. S. Matthews (Tucson, AZ: University of Arizona Press), 27, 921
Britt, D. T., Bell, J. F., Haack, H., & Scott, E. R. D. 1992, Meteoritics, 27, 207
Bus, S. J., & Binzel, R. P. 2002, Icarus, 158, 146
Busarev, V. V., Makalkin, A. B., Vilas, F., Barabanov, S. I., & Scherbina, M. P. 2018, Icarus, 304, 83
Campins, H., Hargrove, K., Pinilla-Alonso, N., et al. 2010, Nature, 464, 1320
Cellino, A., Zappala, V., & Farinella, P. 1989, Icarus, 78, 298
Christou, A. A. 2013, Icarus, 224, 144
Clark, B. E., Binzel, R. P., Ellen S. H., et al. 2011, Icarus, 216, 462
de la Fuente Marcos, C., & de la Fuente Marcos, R. 2013, MNRAS, 432, 31
Desch, S. J. 2007, ApJ, 671, 878
Emery, J. P., Burr, D. M., & Cruikshank, D. P. 2011, AJ, 141, 25
Fornasier, S., Lantz, C., Barucci, M. A., & Lazzarin, M. 2014, Icarus, 233, 163
Fraeman, A. A., Murchie, S. F., Arvidson, R. E., et al. 2014, Icarus, 229, 196
Harris, A. W. 1994, Icarus, 207, 209
Harris, A. W. 1998, Icarus, 131, 291
Hiroi, T., Zolensky, M. E., Pieters, C. M., & Lipschutz, M. E. 1996, Meteor. Planet. Sci., 31, 321
Izidoro, A., de Souza Torres, K., Winter, O. C., & HaghiGHipour, N. 2013, ApJ, 767, 54
Jockers, K., Credner, T., Bonev, T., et al. 2000, Kinematika i Fizika Nebesnykh Tel Supplement, 3, 13
Lantz, C., Clark, B. E., Barucci, M. A., & Lauretta, D. S. 2013, A&A, 554, A138
Lebofsky, L. A. 1980, AJ, 85, 573
Lebofsky, L. A., & Spencer, J. R. 1989, in Asteroids II, eds. R. P. Binzel, T. Gehrels, & M. S. Matthews (Tucson, AZ: Arizona University Press), 128
Lebofsky, L. A., Sykes, M. V., Tedesco, E. F., et al. 1986, Icarus, 68, 239
Licandro, J., Campins, H., Kelley, M., et al. 2011, A&A, 525, A34
Mainzer, A., Grav, T., Masiero, J., et al. 2012, ApJ, 760, L12
Matsuoka, M., Nakamura, T., Kimura, Y., et al. 2015, Icarus, 254, 135
Morbidelli, A., Chambers, J., Lunine, J. I., et al. 2000, Met. Planet. Sci., 35, 1309
Morbidelli, A., Lunine, J. I., O'Brien, D. P., Raymond, S. N., & Walsh, K. J. 2012, Ann. Rev. Earth. Planet. Sci., 40, 251
Moroz, L. V., Fisenko, A. V., Semjonova, L. F., Pieters, C. M., & Korotaeva, N. N. 1996, Icarus, 122, 366
Nugent, C. R., Mainzer, A., Masiero, J., et al. 2015, ApJ, 814, 117
Perna, D., Dotto, E., Barucci, M. A., et al. 2013, A&A, 555, A62
Perna, D., Alvarez-Candal, A., Fornasier, S., et al. 2014, A&A, 568, L6
Perna, D., Barucci, M. A., Ishiguro, M., et al. 2017, A&A, 599, L1
Polishook, D., Jacobson, S. A., Morbidelli, A., & Aharonson, O. 2017, Nature, 1, 0179
Popescu, M., Birlan, M., & Nedelcu, D. A. 2012, A&A, 544, A130
Pravec, P., Harris, A. W., Scheirich, P., et al. 2005, Icarus, 173, 108
Raymond, S. N., & Izidoro, A. 2017, Icarus, 297, 134
Rivkin, A. S., & Emery, J. P. 2010, Nature, 464, 1322
Rivkin, A. S., Brown, R. H., Trilling, D. E., Bell, J. F., & Plassmann, J. H. 2002, Icarus, 156, 64
Rivkin, A. S., Binzel, R. P., Howell, E. S., Bus, S. J., & Grier, J. A. 2003, Icarus, 165, 349
Rivkin, A. S., Trilling, D. E., Thomas, C. A., et al. 2007, Icarus, 192, 434
Sanchez, J. A., Reddy, V., Kelley, M. S., et al. 2014, Icarus, 228, 288
Scholl, H., Marzari, F., & Tricarico, P. 2005, Icarus, 175, 397
Spencer, J. R. 1990, Icarus, 83, 27
Takir, D., & Emery, J. P. 2012, Icarus, 219, 641
Tholen, D. J. 1984, PhD Thesis (Tucson, AZ: University of Arizona)
Vernazza, P., Marsset, M., Beck, P., et al. 2016, AJ, 152, 54
Vilas, F., & Gaffey, M. J. 1989, Science, 246, 790
Vilas, F., Jarvis, K. S., & Gaffey, M. J. 1994, Icarus, 109, 274
Vilas, F., Smith, B., McFadden, L., et al. 1998, Vilas Asteroid Spectra V1.1, eAR-A-3-RDR-VILAS-ASTEROID-SPECTRA-V1.1. NASA Planetary Data System
Vokrouhlický, D., Bottke, W. F., & Nesvorný, D. 2016, AJ, 152, 39
Walsh, K. J., Morbidelli, A., Raymond, S. N., O'Brien, D. P., & Mandell, A. M. 2011, Nature, 475, 206